Journal of the Korean Physical Society, Vol. 59, No. 5, November 2011, pp. 3080∼3088

Determination of the Optical Properties of a Bent Optical Fiber by Using an Automatic Fringe Pattern Analysis

M. A. M. El-Morsy*

Physics Department, College of Science and Humanitarian Studies, Al-Kharj University, Saudi Arabia and Physics Department, Faculty of Science Demietta, Mansoura University, New Demietta, Egypt

H. H. Wahba

Physics Department, Faculty of Science Demietta, Mansoura University, New Demietta, Egypt

(Received 21 June 2011, in final form 16 September 2011)

The automatic multiple-beam Fizeau fringe technique with the aid of the slab model is used to characterize the macroscopic and the microscopic optical parameters of bent optical fiber cladding. The contour line of the interferogram is obtained using a one dimensional Fourier transform. The used mathematical expressions are based on a consideration of refraction of the beam through the liquid/bent fiber interface. The refractive index profile, the induced birefringence profile and the dispersions are studied along the cladding diameter. The influences of bending on the dispersion parameters, such as the oscillation energy E_0 and the dispersion energy E_d, for the optical fiber cladding are investigated. Also, the variations in the molecular polarizability and corresponding parameters are illustrated.

PACS numbers: 78.20.-e
Keywords: Optical fiber, Refractive index profile, Induced birefringence, Fizeau interferometer
DOI: 10.3938/jkps.59.3080

I. INTRODUCTION

The refractive index profile and the birefringence of fibers are important parameters in many fields of applications. The values of the refractive indices of the optical fiber give useful information about the structural parameters of those fibers. Also, they provide information about the microscopic parameters, such as the oscillation energy, the dispersion energy and the molecular polarizability. Some optical sensors and optical communication devices are based on the induced birefringence of optical fibers.

The effect of the mechanically induced residual stress on the refractive index of a single mode optical fiber was studied by Hibino *et al.* [1]. The birefringence was negative for elongation stress. The cutoff wavelength shifted to shorter wavelengths with decreasing refractive index. The relation between the residual stress and the drawing tension was linear.

An isotropic plastic optical fiber becomes a uniaxial fiber as a result of the bending effect. The induced birefringence is linearly proportional to the distance measured from the neutral line [2].

Tai and Rogowski [3] gave a more generalized study that was applicable to all plastic and glass fibers. They observed that, bending leads to a linear increase in the refractive index in the compression part and vice versa. Barlow and Payne [4] measured the stress optic coefficient and its dispersion for twisted optical fiber. They found that the dispersion effect of the photoelastic coefficient couldnot be neglected in fields of applications based on the optical fibers and their birefringence.

The macro bending loss for optical fibers was studied as a function of the bending radius by using the beam propagating method [5,6]. Many different techniques have been applied to determine the refractive index profile and the birefringence profile of fibers [7–12].

T multiple-beam Fizeau fringe system [13–15] is one of the most sensitive and non-destructive techniques used to investigate optical fiber parameters. Numerous authors have investigated the optical properties of fiber by using the manual multiple beam Fizeau interferometer in transmission with mathematical expressions that neglected the refraction of the incident light beam [16,17].

Hamza and coworkers [18–20] derived a mathematical expression to calculate the refractive index of a fiber. The mathematical expression was based on the refraction of the light beam through the fiber. The method based on the refraction consideration gave more accurate results than the methods neglecting the refraction.

The power of multiple-beam Fizeau fringe interferom-

*E-mail: elmorsym@yahoo.com

eter changed dramatically with the introduction of automated methods of detection and analysis of fringe patterns [21–23]. The refractive index profile, the induced birefringence and some guidance parameters of the bent optical fiber were calculated using the automatic Fizeau interferometer and a new mathematical model [24] (slab model). The slab model takes into consideration the refraction of the incident beam by the bent optical fiber. The present paper focuses on automatic determination of the contour line of the multiple-beam Fizeau fringes and then calculates automatically the perturbation of the macro and the microscopic parameters due to the bending process, taking the refraction of the incident beam by the bent optical fiber into consideration.

II. THEORETICAL CONSIDERATIONS

1. Multiple Beam Fizeau Frings Interferometer

The automatic multiple-beam Fizeau fringe interferometer with the aid of the slab model is used for the bent optical fiber characterization. The mechanical bending of the homogenous isotropic optical fiber leads to the appearance of an anisotropy in the bent fiber. The bent optical fiber becomes uniaxial material. This fiber will have different refractive indices in the directions parallel and perpendicular to the fiber optical axis. The refractive indices in the parallel and the perpendicular directions are called $n^{\parallel}$ and $n^{\perp}$, respectively. These refractive index components can be calculated using a monochromatic light beam's components vibrating parallel and perpendicular to the fiber optical axis. The parallel component of the refractive index ($n^{\parallel}$) is affected by the mechanical bending. There are no changes occurring in the other component of the refractive index ($n^{\perp}$) due to the bending . The mechanical bending leads to a compression in the inner region and an extension in the outer region of the bent fiber. The refractive index increases in the compressed region and decreases in the extended region so that the induced birefringence will be positive in the compressed region and it will be negative in the extended region.

The slab model [24] divides the bent optical fiber into a great number of slabs. These slabs are perpendicular to the bending radius (see Fig. 1). Every slab is characterized by its own refractive index. The incident beam suffers refractions due to its path across the slabs of the bent optical fiber. Figure 2 shows the path of the incident light beam across k slabs and its angles of incidence and refraction. This mathematical model is based on the refraction consideration of the used light beam across the fiber/liquid interface, as well as the refraction across the slabs of the bent fiber. The incident light beam will enter the bent fiber at slab number j and leave the fiber from slab number $j+k-1$. The refractive index of slab number j is n_j. The angles of incidence and refraction are θ_{ij} and θ_{rj}, respectively. The incident beam will strike the fiber at a distance x_{ij} and leave the fiber at a distance x_{ej+k-1}, with these distances being measured from the fibers center. The refracted beam enters slab number $j+1$ at distance x_{j+1} and so on. The optical path difference of the refracted beam through k slabs can be calculated using the following recurrence relation:

$$\frac{\lambda Z_{jj+k-1}}{2B} = \left[n_j \frac{x_{ij}-x_{j+1}}{\sin(\theta_{ij}-\theta_{rj})} + \sum_{l=j+1}^{j+k-2} n_l \frac{x_l - x_{l+1}}{\cos(\theta_{rl})} + n_{j+k-1} \frac{x_{j+k-1}-x_{ej+k-1}}{\cos(\theta_{rj+k-1})} \right] - n_L \left[\frac{x_{ij}-x_{j+1}}{\tan(\theta_{ij}-\theta_{rj})} + \sum_{l=j+1}^{j+k-2} [x_l - x_{l+1}\tan\theta_{rl}] + [(x_{j+k-1}-x_{ej+k-1})\tan\theta_{rj+k-1}] \right], \quad (1)$$

where λ is the wavelength of the incident light beam, Z_{jj+k-1} is the shift of the incident light beam through its path in k slabs and B is the interfringe spacing. The summation index takes the values $l = j+1, j+2, \ldots, j+k-2$. The bent optical fiber immerges in a liquid of refractive index n_L.

The automatic Fizeau fringe interferometer with the aid of a prepared computer program based on the slab model is used to calculate the refractive index profile of the bent optical fiber. The refractive indices along the bent optical fibers diameter at different wavelengths are used to calculate the dispersion parameters. Also, the molecular polarizability and the corresponding parameters can be obtained.

2. Macroscopic and Microscopic Parameters of the Bent Optical Fiber

The dispersive characterization of the optical fiber material can be described using the Sellmeier dispersion formula (*cf.* Ref. 25) for the refractive index:

$$n^2 - 1 = \sum_j \frac{A_j \lambda^2}{\lambda^2 - \lambda_{0j}^2}, \quad (2)$$

where λ_{0j} and $A_j = (Ne^2\lambda_{0j}/\,(2\pi c)^2 \epsilon_0 m)$ are the resonant wavelength and the magnitude of the j^{th} resonance, e and m are the electron charge and the electron mass, respectively, N is the number of molecules per unit volume,

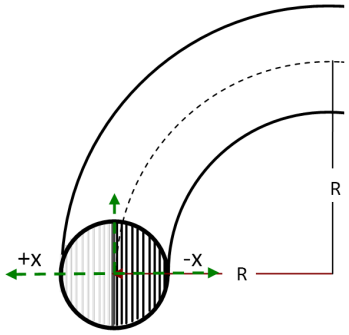

Fig. 1. (Color online) Schematic diagram of the bent fiber cross section.

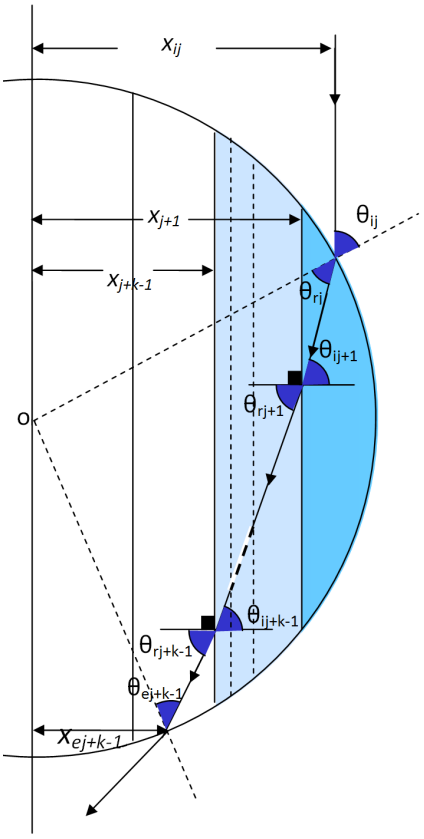

Fig. 2. (Color online) Ray tracing cross k slabs.

c is the velocity of light and ϵ_0 is the dielectric permittivity of free space. The refractive index will decreases as wavelength increases for transparent linear isotropic dielectric materials if all electrons have the same natural frequency ω_0. This leads to that the dispersion relation taking the following form [26]:

$$n^2 - 1 = \frac{Ne^2}{\varepsilon_0 m} \frac{1}{\omega_0^2 - \omega^2}, \tag{3}$$

where ω is equal to $(2\pi c/\lambda)$.

Multiplying the right side of Eq. (3) by $(h/2\pi)^2/(h/2\pi)^2$, one can get

$$n^2 - 1 = \frac{F}{E_0^2 - E^2}, \tag{4}$$

where F is the oscillator strength ($F = (\mathrm{Ne^2h^2})/(4\pi^2\epsilon_0 m)$) and h is the Planck constant. E_0 and E are the oscillator energy and the incident beam energy, respectively.

Wemple and DiDomenico [27] represented an empirical relation between the oscillator strength F and the parameter E_d (dispersion energy), which measured the strength of inter-band optical transition as follows:

$$E_d = \frac{F}{E_0}. \tag{5}$$

Using Eq. (5) in Eq. (4), one gets

$$n^2 - 1 = \frac{E_d E_0}{E_0^2 - E^2}. \tag{6}$$

This equation is applicable in a wide range of crystalline and amorphous solids [28]. Using Eq. (6), it is easy to calculate E_0 and E_d. The values of E_0 and E_d describe the refractive index dispersion data of a given material. The dispersion energy E_d depends on the coordination number and the chemical valency [27,28]. These with the aid of the localized molecular theory of optical transition lead to an understanding of the behavior of the refractive index [27].

The molecular field E_m defines the electric field at a molecular position in the dielectric. This field is produced by all external sources and by all polarized molecules in the dielectric with the exception of the molecule at the point under consideration. Lorentz estimated the relation between the E_m and the external field E and the polarization P to be as follows [29]:

$$E_m = E + \frac{1}{3\varepsilon_0} P. \tag{7}$$

The dipole moment p_m of a molecule is proportional to the polarizing field E_m:

$$P_m = \alpha E_m, \tag{8}$$

where α is the molecular polarizability and is defined as the ratio between the dipole moment of a molecule and the polarizing field [29]. Some authors have called α the mean polarizability [30]. The relation between the refractive index and the molecular polarizability can be expressed as:

$$\alpha = \frac{3\varepsilon_0}{N} \frac{n^2 - 1}{n^2 + 2}. \tag{9}$$

This equation is known as the Clausius-Mossotti equation [31] and represents the relation between the macroscopic parameter n (the refractive index) of the dielectric and its microscopic parameters α and N.

Equation (9) can be rewritten in the following form [32]:

$$\alpha_i = \frac{3\varepsilon_0}{N}\frac{n_i^2-1}{n_i^2+2}, \tag{10}$$

where n_i and α_i are the refractive index and the molecular polarizability components when one use monochromatic light vibrating in the direction i (parallel $\parallel$ or perpendicular $\perp$ to the fibers axis, respectively. Also, the polarizability per unit volume, Φ_i, can be written as follows [32]:

$$\Phi_i = \frac{n_i^2-1}{n_i^2+2}. \tag{11}$$

The polarizability per unit volume increases as the refractive index increases and vice versa.

The polarizability of a mole of the dielectric M_i can be defined as [30]:

$$M_i = \frac{N_A\alpha_i}{3\varepsilon_0} = \frac{m_w}{\rho}\frac{n_i^2-1}{n_i^2+2}, \tag{12}$$

where m_w and ρ are the molecular weight and the density, respectively. N_A is Avogadro's number, and M_i is the molar polarizability of a dielectric. The refractive index depends on the density of the material.

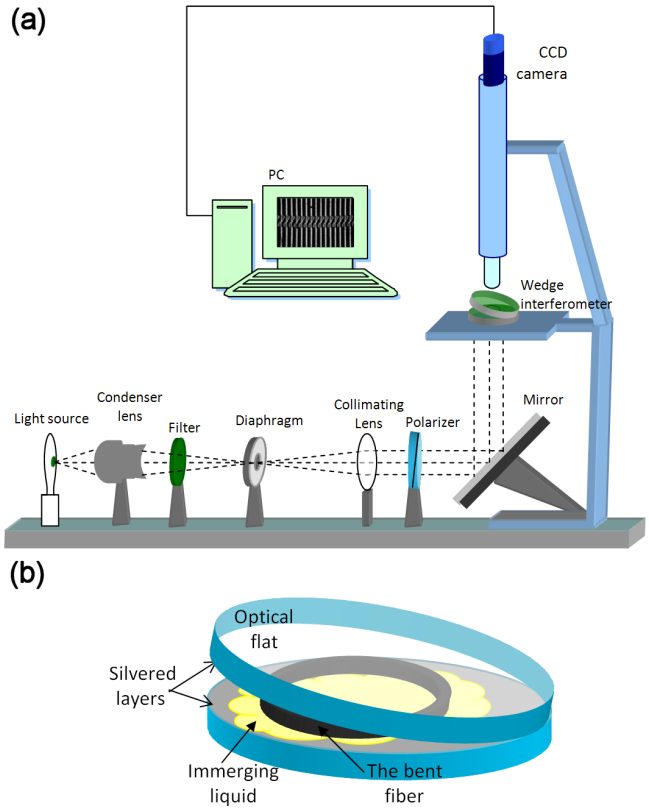

Fig. 3. (Color online) Schematic diagrams of (a) the Fizeau technique and (b) the wedge interferometer.

III. EXPERIMENTAL TECHNIQUE

The Fizeau interferometer is used to determine the refractive index profile of fibers as well as the structural parameters of fibers, with high accuracy [33]. In our study, we use the automatic Fizeau interferometer in transmission. Figure 3(a) illustrates the Fizeau interferometer setup. The Hg lamp is used as a light source of different wavelengths. To obtain a parallel beam of polarized monochromatic light we used suitable optical components. The used optical components are a condensing lens, a collimating lens and the desired interference filter. To select a certain component of the monochromatic light beam we used a polarizer. Now, one can obtain a polarized monochromatic parallel beam of light. Figure 3(b) shows the wedge interferometer. It consists of two circular optical flats with a 5 cm diameter, a 1 cm thickness and a ± 0.01 μm flatness. The optical flats are coated on the inner face with pure silver. The silvered layer has a reflectivity an about 75% and a transmittance an about 22%. A special holder was prepared to contain the optical flats to form the wedge interferometer. The wedge contains the bent optical fiber immersed in a suitable liquid ($n_L = n^{\perp}$). One can get a sharp interference pattern perpendicular to the fiber by adjusting the wedge angle and the gap thickness between the flats. We use a microscope to observe the pattern. A CCD camera attached to the microscope was used to capture the produced interferogram. The CCD was connected to a PC through a frame grabber. A prepared image processing program was used to obtain the contour line of the fringe pattern and then to calculate the refractive index profile of the used fiber.

IV. RESULTS AND DISCUSSION

The bent plastic optical fiber was studied using the multiple-beam Fizeau interferometer in transmission. Figure 4(a) shows an interferogram of multiple-beam Fizeau fringes when we used a monochromatic light of wavelength $\lambda = 535.1$ nm without a polarizer. The bending radius R was equal to 8.95 mm. This bent optical fiber was immersed in a liquid of refractive index 1.4603. The bending effect clearly appeared along the optical fiber's cladding. The shift inside the fiber cladding had bow shape. Referring to the interferogram show in Fig. 4(b) one can note that, when the used monochromatic light vibrated perpendicular to the fiber's axis, the shift along the fiber was not affected by the bending. The bending effects appear in the shift along the fiber's cladding when the light vibrated parallel to the fiber's axis (see Fig. 4(c)).

The refractive index profile was calculated, considering the refraction of the light beam through the fiber, by

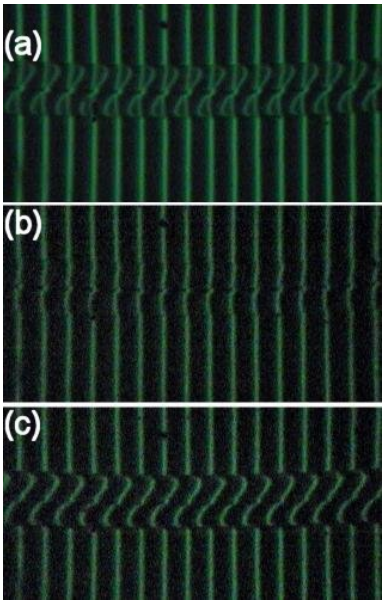

Fig. 4. (Color online) Interferograms of the multiple beam Fizeau fringes when using (a) an unpolarized light beam, (b) light vibrating perpendicular to the fiber axis and (c) light vibrating parallel to the fiber axis, respectively.

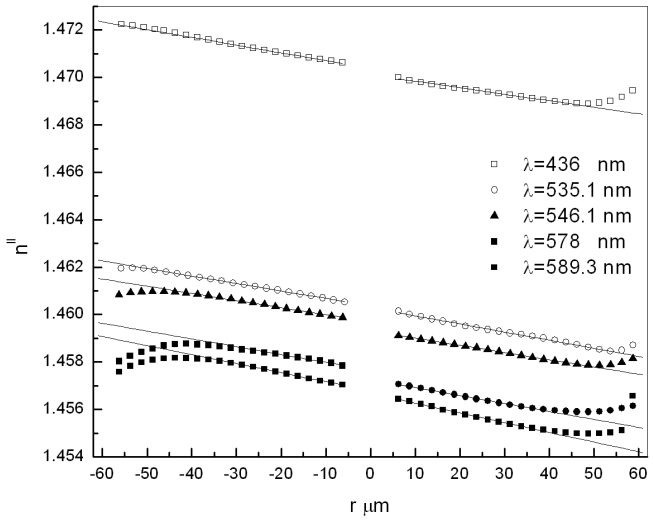

Fig. 5. Refractive index profile $n^{\parallel}$ at different wavelengths of λ = 436, 535.1, 546.1, 578, and 589.3 nm.

using Eq. (1) (slab model [24]). We prepared a special program to detect the contour line of the fringe shifts by using a one-dimensional Fourier transform [21]. Then, the refractive index profile was calculated with an accuracy of about $\pm 1 \times 10^{-4}$. Figure 5 shows the refractive index profile $n^{\parallel}$of the optical fiber's cladding when using the parallel component of the used light at different wavelengths λ = 436, 535.1, 546.1, 578, 589.3 nm, respectively. The bending effect on the bent optical fiber can be summarized in two effects; the first is a compression and the second is a tension around the fiber's center.

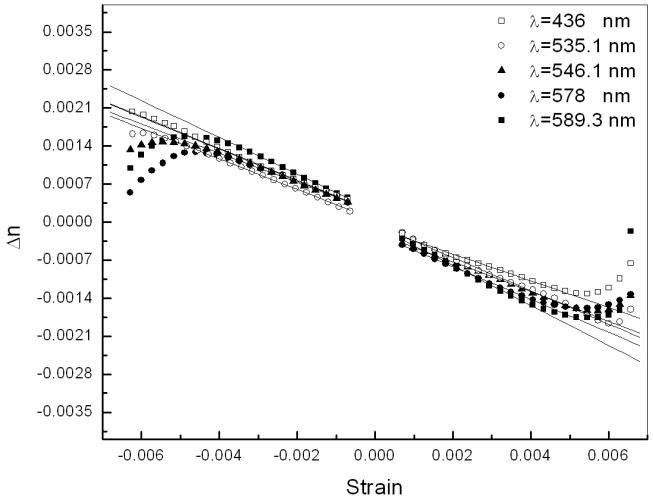

Fig. 6. Induced birefringence-strain relation at different wavelengths λ = 436, 535.1, 546.1, 578, and 589.3 nm for the bent optical fiber.

Compression occurs in the inner cladding region at $x < 0$, and tension occurs in its outer region at $x > 0$, where x is along the x-axis across the fiber's radius. The refractive index $n^{\parallel}$ is larger in the compression region and is smaller in the tension region compared to $n^{\perp}$.

Figure 5 illustrates that the behavior of the refractive index profile ($n^{\parallel}$) through the optical fiber's radius is linear, but the refractive index profile ($n^{\parallel}$) near the fiber's border goes toward a liquid refractive index. This may be a result of the thickness of the optical fiber, which decreases in the border region, leading to an ascendancy of the optical path through the liquid inside the fiber. Then, the fluctuations in the refractive index of the fiber's cladding its and birefringence are linear in the mechanical strain [1,2].

The induced birefringence ($\Delta n = n^{\parallel} - n^{\perp}$) of the optical fiber's cladding is a result of the bending. The mechanical strain across the fiber's radius can be calculated using the linear relation (strain = x/R), where R is the radius of curvature. The induced birefringence-strain curve is given in Fig. 6 at different wavelengths λ = 436, 535.1, 546.1, 578, 589.3 nm. The relation between the induced birefringence and the strain is linear across the cladding, except in the border regions, due to the effect of the liquid. The induced birefringence increases in the compression region and decreases in the extension region.

Equation (6) represents the relation between the refractive index and the dispersion, oscillation and photon energies. Equation (6) is used to determine the values of the dispersion energy E_0 and the oscillation energy E_d. Figures 7(a) and 7(b) give the plots of $1/(n^2 - 1)$ versus E^2 in the tension and the compression regions at x = 5, 30, 45, and 60 μm and x = –5, –30, –45, and –60 μm, respectively. According to Eq. (6) the fitting are straight lines at any point x along the bent optical fiber

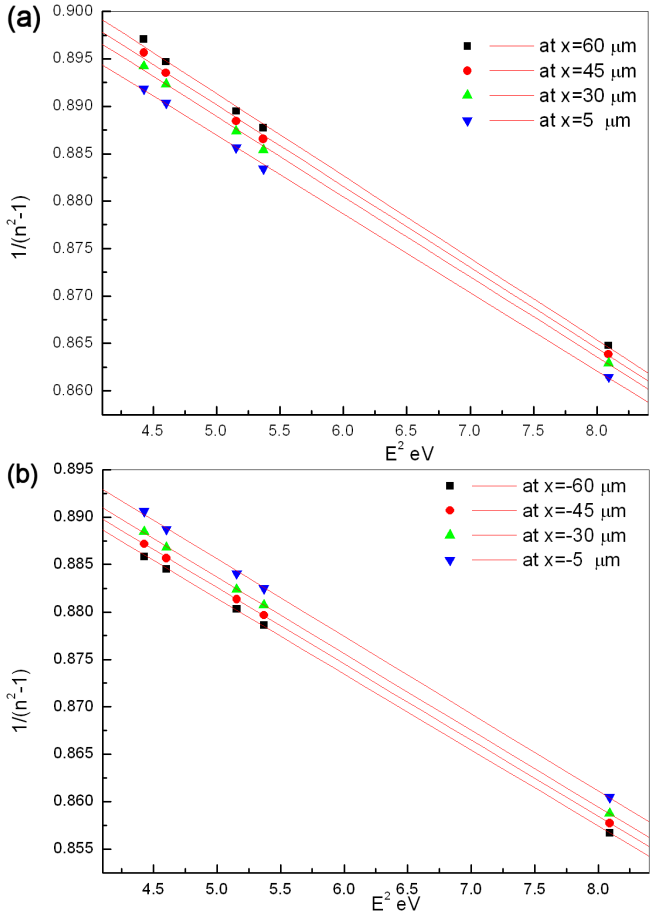

Fig. 7. (Color online) (a) Relation between $1/(n^2-1)$ and E^2 at different values of x along the the bent fiber cladding in the tension region. (b) The same as (a), but in the compression region.

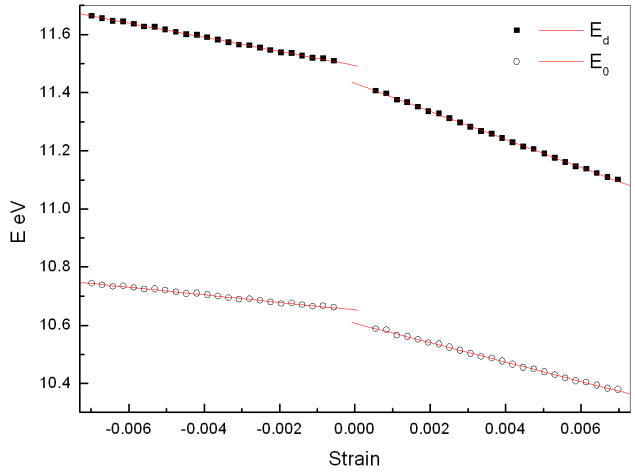

Fig. 8. (Color online) Relation between the strain and E_0, E_d along the fiber cladding under bending and fittings in the tension and the compression regions.

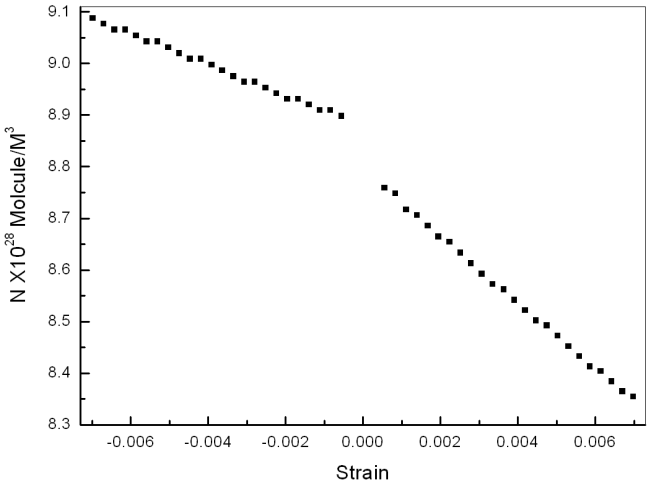

Fig. 9. Relation between the number of molecules and the strain in the tension and the compression regions.

cladding. The slope of the fitted line and its intercept are $(1/E_0E_d)$ and (E_0/E_d), respectively.

Figure 8 describes the relation between the macroscopic strain, the calculated dispersion energy E_d and oscillation energy E_0 along the bent optical fiber's cladding. The energies E_d and E_0 are linearly proportional to the strain in the tension and the compression regions. The accuracies of the measurements of E_0 and E_d are ± 0.0452, ± 0.0539 eV, respectively. The oscillation and the dispersion energies of the bend-free optical fibers are 10.6276 ± 0.0452 and 11.4610 ± 0.0539 eV, respectively. The bending of the optical fiber's cladding causes a macroscopic strain (x/R). The bending also leads to a microscopic strain, which leads to a variations in the oscillation and the dispersion energies. The microscopic strain stretches or compresses the bonds between the atoms of the bent optical fiber's cladding. The microscopic stain is proportional to the macroscopic strain. The dispersion and the oscillation energies decrease along the bent optical fiber cladding as strain increases in the tension region where the bonds will be stretched. On the other hand, these energies increase in the compression region where the bonds be compressed along the bent cladding. These experimental results coincide with the hypothesis of the inverse proportionality of E_0 with the bond length u between atoms, as proposed by Wemple [34]. He stated that the relation between the oscillator energy E_0 and the bond length u is described by the relation $E_0\alpha\ \mathrm{u}^{-2.5}$. The bond compression increases the oscillator energy E_0, and the bond extension decreases E_0. Changes in the refractive index can be takes place due to the effects of compression and tension on E_0 and E_d, which increase with compression and decreases with tension. The optical fiber's bending leads to fluctuations in the dispersion and oscillation energies. Due to these fluctuations, the refractive index will change along the fiber's diameter.

The bending affects the number of molecules per unit volume along the bent optical fiber's cladding. Tension increases distances between the molecules contained in

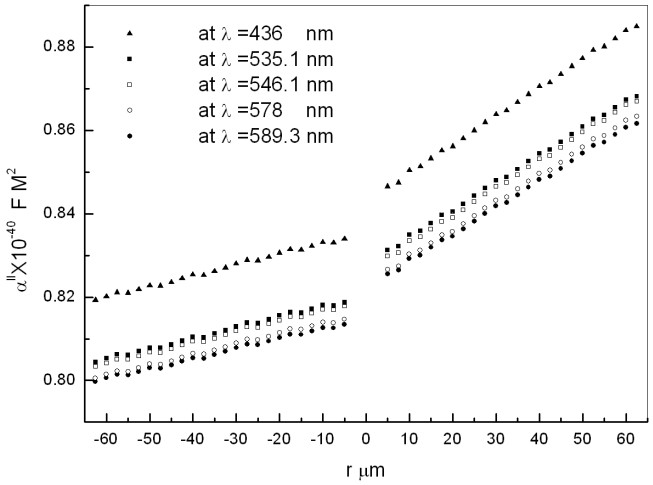

Fig. 10. Molecular polarizability at different wavelengths in the tension region and the compression region.

the bent optical fiber's cladding and vice versa for compression. The number of molecules per unit volume, N, can be calculated using the relation between E_o, E_d, and the oscillator strength F (Eq. (5)). The number of molecules per unit volume will decrease as bonds stretch in the tension region. On the other hand, it will increase as bonds compress in compression regions. Figure 9 shows these results. The ratio m_w/ρ can give the molar volume V_m, which is given by $V_m = (m_w/\rho) = (N_A/N)$ [30]. The molar volume of the bent optical fiber will increase in the extension region and decrease in the compression region. Consequently, the number of molecules per unit volume, N, will be increase when the bent optical fiber compresses and vice versa. The density decreases in the tension region and increases in the compression region. The refractive index is proportional to the bent optical fiber's density. These results coincide with the hypothesis that the refractive index of the bent optical fiber will increase with compression and decrease with tension.

One can use Eq. (10) to determine the molecular polarizability components at any point along the bent optical fiber's cladding. Figure 10 shows the molecular polarizability $\alpha^{\parallel}(x)$, at different wavelengths $\lambda = 436$, 535.1, 546.1, 578, and 589.3 nm. The parallel component of the molecular polarizability $\alpha^{\parallel}(x)$ increases with tension and decreases with compression.

The macroscopic parameter $\Phi^{\parallel}(x)$ (the polarizability per unit volume) along the bent fiber's cladding with different wavelengths is shown in Fig. 11. The polarizability per unit volume $\Phi^{\parallel}(x)$ decreases as the used wavelength increases. The polarizability per unit volume $\Phi^{\parallel}(x)$ decreases in the tension region as refractive index decreases and vice versa in the compression region.

Using Eqs. (10) and (11) and $V_m = (m_w/\rho) = (N_A/N)$, one can obtain the relation between the molar volume and the microscopic parameter α_i and the macroscopic parameter Φ_i, which can be writen as $\Phi_i = (N_a\alpha_i/3\varepsilon_0 V_m) = \left(\left(n_i^2-1\right)/\left(n_i^2+2\right)\right)$. The polarizability per unit volume is inversely proportional to the molar volume, consequently, the refractive index increases as the molar volume decreases. This occurs when the bent optical fiber is compressed and vice versa. According to

Table 1. The molecular polarizability, the molar polarizability, and the polarizability per unit volume of the studied optical fiber.

Wavelength (nm)	$\alpha^{\perp} \times 10^{-40}$ FM^2	$M^{\perp} \times 10^{-3}$ KgM^3	$\Phi^{\perp}$
436	0.84023	1.98294	0.27911
535.1	0.82503	1.94706	0.27406
546.1	0.82373	1.94401	0.27363
578	0.8206	1.93662	0.27259
589.3	0.81946	1.93392	0.27221

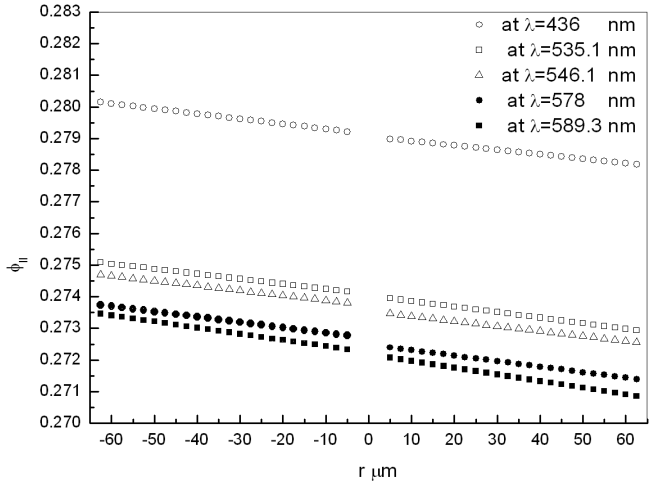

Fig. 11. Polarizability per unit volume $\Phi_{\parallel}$ along the bent fiber cladding at different wavelengths.

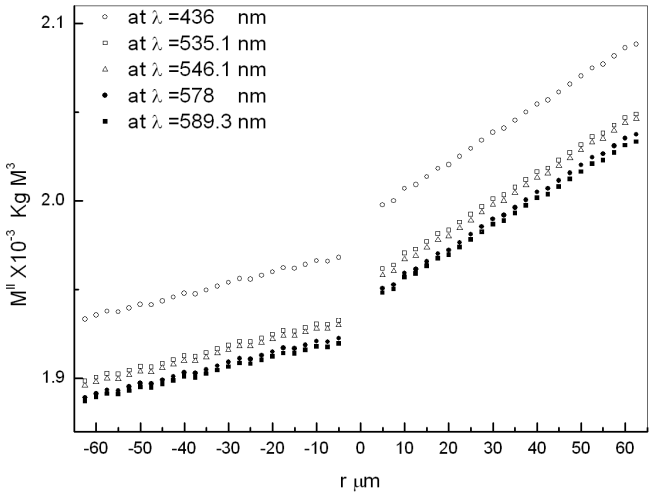

Fig. 12. Molar polarizability $M^{\parallel}$ along the bent fiber cladding at different wavelengths.

the above equation, the $\Phi^{\parallel}(x)$ is inversely proportional to the molar volume and to refractive index $n^{\parallel}$.

The molar polarizabilities $M^{\parallel}(x)$ and $M^{\perp}(x)$ can be calculated using Eq. (12). Table 1 summarizes the characteristic parameters of the bend-free optical fiber: the molecular polarizability $\alpha^{\perp}(x)$, the molar polarizability $M^{\perp}(x)$ and the polarizability per unit volume $\Phi^{\perp}(x)$ at different wavelengths λ = 436, 535.1, 546.1, 578, and 589.3 nm.

$M^{\parallel}(x)$ along the bent fiber cladding is given in Fig. 12 for different wavelengths. The molar polarizability decreases as the used wavelength increases. The molar volume increases as tension increases and decreases as compression increases. Consequently, the $M^{\parallel}(x)$ increase in the tension region and deceases in the compression region.

V. CONCLUSION

A computerized Fizeau interferometer with a slab model is used to calculate the macroscopic and the microscopic parameters for bent optical fiber cladding with high accuracy. The considered macroscopic parameters are the refractive index profile, the induced birefringence, the molar polarizability and the polarizability per unit volume. The accuracy of the calculations is increased due to consideration of the refraction of the incident light beam at the liquid/fiber interface. Microscopic parameters such as the dispersion energy, the oscillation energy and the molecular polarizability are obtained. All these parameters ware determined along the cladding of the bent optical fiber.

From this study one can conclude the following:

1. The dispersion parameters (E_0, E_d) are affected by mechanical bending of the optical fiber cladding. The dispersion parameters are increased in the compression region as a result of bond compression and are decreased in the extension region. Consequently, the refractive index and the induced birefringence are increased in the compression region and are decreased in the extension region.

2. The polarizability per unit volume depends on the refractive index along the bent fiber cladding, but the molar polarizability increases in the tension region as a result of the molar volume increase in that region and is decreased in the compression region.

3. The molecular polarizability is inversely related to the number of molecules per unit volume which increase in the compression region and decreases in the tension region so that the molecular polarizability decreases in the compression region and increases in the extension region along the bent optical fiber cladding. These parameters depend on the wavelength of the incident beam. The polarizabilities inversely depend on the wavelength.

4. The automated Fizeau interferometer is a good tool to characterize the macroscopic and the microscopic parameters of a bent optical fiber.

ACKNOWLEDGMENTS

The authors would like to thanks Prof. A. A. Hamza for his encouragement throughout this work. Also, we would like to express our deep thanks to Prof. T. Z. N. Sokkar for his useful discussions.

REFERENCES

[1] Y. Hibino, F. Hanawa and M. Horiguchi, J. Appl. Phys. **65**, 30 (1989).
[2] J. Zubia and J. Arrue, IEE Proc.: Optoelectron. **144**, 397 (1997).
[3] H. Tai and R. Rogowski, Opt. Fiber Technol. **8**, 162 (2002).
[4] A. J. Barlow and D. N. Payne, IEEE J. Quantum Electron. **QE-9**, 834 (1983).
[5] H. Vendeltorp-Pommer and J. H. Povlsen, Opt. Commun. **75**, 25 (1990).
[6] J. Yamauchi, M. Ikegaya and H. Nakano, IEE Proc-J **139**, 201 (1992).
[7] A. A. Hamza, A. M. Ghander and M. A. Mabrouk, J. Opt. A: Pure Appl. Opt. **1**, 71 (1992).
[8] W. A. Ramadan, J. Opt. A: Pure Appl. Opt. **2**, 234 (2000).
[9] N. A. Paraire, N. Moresmau, S. Chen, P. Dansa and F. Bertrand, Appl. Opt. **36**, 2545 (1997).
[10] T. Z. N. Sokkar, M. A. Mabrouk and H. F. El Bawab, J. Opt. A: Pure Appl. Opt. **1**, 64 (1999).
[11] A. A. Hamza, I. M. Fouda, T. Z. N. Sokkar and M. A. El Bakary, J. Appl. Polym. Sci. **69**, 1495 (1998).
[12] B. Ibarra-Escamilla and E. A. Kuzin, Opt. Lasers Eng. **39**, 635 (2003).
[13] A. A. Hamza, T. Z. N. Sokkar, M. A. El-Morsy, M. I. Raslan and A. M. Ali, Opt. Commun. **283**, 1684 (2010).
[14] A. A. Hamza, T. Z. N. Sokkar, K. A. El-Farahaty and H. M. El-Dessouky, Opt. Lasers Eng. **41**, 261 (2004) .
[15] A. A. Hamza, T. Z. N. Sokkar, M. A. Mabrouk and M. A. El-Morsy, J. Appl. Polym. Sci. **77**, 3099 (1999).
[16] F. El-Diasty, J. Opt. A: Pure Appl. Opt. **4**, 575 (2002).
[17] A. A. Hamza, T. Z. N. Sokkar and M. A. El-Bakary, Opt. Laser Technol. **38**, 162 (2006).
[18] A. A. Hamza, T. Z. N. Sokkar, M. A. Mabrouk, A. M. Ghandar, W. A. Ramadan, J. Opt. A: Pure Appl. Opt. **3**, 943 (1994).
[19] A. A. Hamza, T. Z. N. Sokkar, M. A. Mabrouk, M. A. Ghandar and W. A. Ramadan, J. Opt. A: Pure Appl. Opt. **4**, 161 (1995).
[20] A. A. Hamza, T. Z. N. Sokker, M. A. El-Morsy and M. A. E. Nawareg, Opt. Commun. **282**, 27 (2009).
[21] M. A. El-Morsy, T. Yatagai, A. A. Hamza, M. A. Mabrouk and T. Z. N. Sokkar, J. Appl. Polym. Sci. **85**, 475 (2002).

[22] M. A. El-Morsy, T. Yatagai, A. A. Hamza, M. A. Mabrouk and T. Z. N. Sokkar, Opt. Lasers Eng. **38**, 509 (2002).
[23] M.A. El-Morsy, K. Harada, M. Itoh and T. Yatagai, Opt. Laser Technol. **35**, 223 (2003).
[24] T. Z. N. Sokkar, M. A. El-Morsy and H. H. Wahba, Opt. Commun. **281**, 1915 (2008).
[25] J. A. Buck, *Fundamental of Optical Fibers* (Wiley-Interscience Publication, 1995), p. 17.
[26] S. A. Akhmanov and S. Yu. Nikitin, *Physical Optics* (Clarendon Press Oxford, 1997), p. 106.
[27] S. H. Wemple and M. DiDomenico, Phys. Rev. B. **3**, 1338 (1971).
[28] S. H. Wemple, D. A. Pinow, T. C. Rich, R. E. Jaeger and L. G. Van Uitert, J. Appl. Phys. **44**, 5432 (1973).
[29] J. R. Reitz, F. J. Milford and R. W. Christy, *Foundations of Electromagnetic Theory* (Addison-Wesley Publishing Company, 1993).
[30] M. Born and E. Wolf, *Principle of Optics* (Cambridge University Press, 1999), p. 92.
[31] B. Tareev, *Physics Of Dielectric Materials* (Mir Publishers, Moscow, 1979).
[32] M. A. Mabrouk and M. A. Shams-Eldin, J. Opt. A: Pure Appl. Opt. **5**, 929 (1996).
[33] N. Barakat and A. A. Hamza, *Interferometry of Fibrous Material* (Adam Hilger, Bristol, New York, London, 1990), p. 55.
[34] S. H. Wemple, J. Chem. Phys. **67**, 2154 (1977).